Proceedings of the 1998 IEEE
International Conference on Robotics & Automation
Leuven, Belgium • May 1998

Robotic Deployment of Electro-Magnetic Sensors for Meteorite Search

Liam Pedersen
The Robotics Institute
Carnegie Mellon University
Pittsburgh PA 15213, USA
http://www.cs.cmu.edu/~pedersen

Abstract

This paper describes the development and implementation of a combined metal and magnetic sensor suite for the detection of meteorites from a mobile robot. The relative disposition of the sensors and the overall configuration of the sensor suite with respect to the rover are such that clean measurements are achieved and interference is minimized. We validated the combined electromagnetic sensors in laboratory and field tests on a variety of stony and iron meteorites. Experiments have shown that both sensing modalities (eddy current and magnetic) are necessary to achieve comprehensive readings from meteorites. The sensors have detected meteorites smaller than 2 cm in size. The sensor suite is configured to allow in-situ, autonomous calibration of the sensors and to mitigate noise from the electrical components of the robot that deploys them. We have evaluated the sensors during the robotic traverse of the Atacama Desert in the summer of 1997, by the Nomad rover. A ruggedized variant of the system described here will be used for autonomous search of meteorites in Antarctica in the 1998 field season.

Introduction

The Antarctic continent is an ideal place to find meteorites. More than half of all meteorites found were recovered there. Moreover, the pristine conditions maximize the scientific values of the meteorites. Since the discovery of possible evidence of life in the Martian meteorite ALH84001, recovered from Antarctica, interest has further intensified.

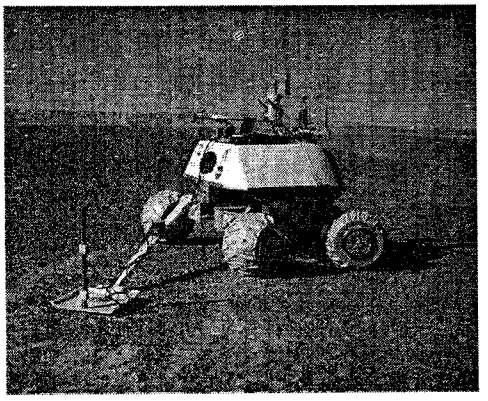

Figure 1 Nomad robot with deployed sensors.

Currently this task is done visually by a team of human searchers who systematically search the blue ice fields and Antarctic moraines. Time restrictions make it uneconomical for them to search snow-covered ice fields with metal detectors or magnetometers to locate buried meteorites. A continuously operating autonomous robot with a wide sensor array would more efficiently search such areas and nicely complement the current collection effort.

This paper describes field tests in Pittsburgh and the Atacama desert (Chile) of a metal detector (eddy current sensor) and magnetometer suite deployed on the Carnegie Mellon University Nomad robot (Figure 1). This robot is a prototype semi-autonomous teleoperated planetary rover, developed for the remote exploration of hostile environments, such as Antarctica, the Moon and Mars.

Test areas in Pittsburgh and the Atacama were seeded with a variety of stony and iron meteorites. The rover then dragged the sensors, mounted on a sliding platform pulled behind the vehicle, over the meteorites. In a subsequent test, remote operators at NASA's Ames Research Center (California) used sensor data obtained during a run in the Atacama to locate a (planted) meteorite and brought the rover around for a visual confirmation.

The purpose of this paper is to describe the analytical and experimental work associated with the robotic deployment of metal detectors and magnetometers for meteorite detection. Deployment of these sensors in the field introduces some unique issues, notably vehicular interference and sensor calibration.

Magnetic Field Measurement

There exist two types of magnetometers: vector sensors and total field sensors. The former (which includes fluxgate sensors, optical fiber interferometers, Hall effect sensors and SQUID's) measure a single component of the magnetic field vector. The latter (which include all magnetic resonance magnetometers) measure the magnitude, but not direction, of the field.

The magnetic field near an object of interest is given by $\vec{B}_t = \vec{B} + \vec{B}_E$, where $\vec{B}$ is the (secondary) field associated with the object, and $\vec{B}_E$ the (primary) ambient field due to the earth and other sources.

The advantage of a total field magnetometer is that its output is largely independent of the sensor orientation. Unfortunately, many of these sensors must be kept roughly aligned with the ambient field to operate. This is not practical for a robotically deployed system.

If the primary field is larger than the secondary, then, to first order, a total field sensor measures the magnitude of the primary field plus the magnitude of the projection of the secondary field onto the primary. Hence, a secondary field perpendicular to the primary will not be detected by this sensor.

The output of a vector magnetometer varies with orientation, and in direct proportion to the total field strength. A sensor operating in a large primary field (such as the Earth's) is particularly sensitive, as the variations may equal or exceed the secondary field due to the object of interest. Typical systems deployed on a robotic vehicle will be subject to rapid and unpredictable orientation changes.

A standard solution to this problem is to use two precisely aligned vector sensors spaced some distance apart, and measure the field difference. This is known as a gradiometer configuration. The disadvantage from a robotic standpoint is the need to keep the sensors precisely aligned along the same axis.

Three vector sensors can be placed orthogonally to measure the full vector field at a point. The field magnitude can be calculated from this, and will be orientation invariant provided the sensors have zero offset and identical scaling. Assuming the secondary field to be localized, another 3-axis sensor located beyond its influence can be used to predict the primary field at the first sensor. The full secondary field can then be inferred.

Magnetic Fields of Meteorites

The secondary field associated with ferrous objects itself consists of two components: an induced field produced by the interaction of the object with the primary field, and that due to the permanent, or remnant, magnetization of the object.

Approximately 90% of all meteorites, including the so-called stony meteorites, contain significant amounts of metallic iron and nickel, both ferromagnetic materials, and so should have induced magnetization.

The magnetic field of several meteorite samples was measured with a Caesium vapor total field magnetometer at the Defense Research Establishment Suffield (DRES) "foam dome" facility in Canada. Measurements were taken at regular intervals on a plane above the samples (Figure 2).

Some of the stony meteorites had fields up to 9 times stronger than that predicted for the same mass of unmagnetized iron by a model developed at DRES. Furthermore, when turned upside down, the field of many meteorites is a direct inversion of the former field. These facts suggest a strong remnant magnetization in the three stony meteorites tested, and a moderate remnant field for a small iron meteorite. The presence of significant remnant magnetization means that they have larger fields and can therefore be detected at a greater distance than the equivalent amount of unmagnetized iron.

Laboratory detection distances varied from 13cm (small iron meteorite) to approximately 25cm (Carraweena stony meteorite). Deviations of total field strength from the ambient geomagnetic field ranged from 50nT (iron meteorite at 11cm distance) to 90nT (Carraweena at 19cm). However, it should be noted that

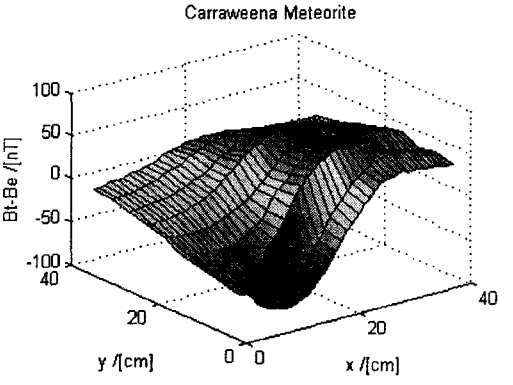

Figure 2 Total magnetic field on plane above meteorite

the meteorites available for testing were large specimens found in Australia, and not necessarily representative of all those typically found in Antarctica, with the exception of the small iron fragment.

Antarctic rocks were also tested. They exhibited negligible magnetization (about 10nT peak for one sample, 20 times less than the predicted field of the same amount of iron).

By comparison, the Earth's field varies from 30,000nT at the magnetic equator to 100,000nT at the magnetic poles It is relatively constant over distances of several hundred meters (the magnetic field gradient is ~ 10 nT/km) and, barring magnetic storms, does not change significantly over short time scales [2].

Robotic Sensor Deployment

Noise and calibration are significant issues in the robotic deployment of magnetic and eddy current sensors.

Electric motors in the wheels and vehicular iron contributed significantly to the ambient magnetic field. Computers, switching mode power supplies and radio communications equipment generated substantial RF interference. Experience proved the eddy current sensor to be particularly sensitive to the latter. For example, it would saturate whenever VHF radios were used by personnel in the robot vicinity. Finally, the sensors themselves generate interference.

A field robotic vehicle is expected to operate for an extended duration in potentially harsh conditions. Vibrations, shock and temperature extremes can change or misalign sensors over time. For example, one of the magnetometers deployed in the Atacama developed a large zero offset in one channel that, uncorrected, greatly degraded the results. Field re-calibration with minimal or no human involvement is obviously desirable.

Finally, the vehicle and sensor platform is seldom stable. For sensors to be useful, signals that are relatively invariant under attitude variations must be obtained, otherwise every object causing the sensor platform to tilt might register as a ferrous object.

The sensors were mounted on a non-metallic sliding platform dragged 8 ft behind Nomad so as to minimize vehicular interference. The sensor coil of a pulse induction eddy current sensor (located as close to the ground as possible) and two 3-axis fluxgate magnetometers were rigidly mounted on the platform:

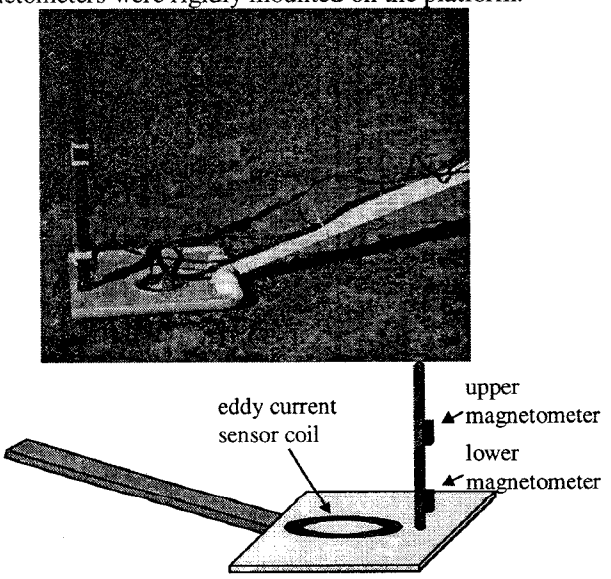

Figure 3 Sensor platform

The 7 sensor channels were each sampled at 800Hz (magnetometers have 400Hz passband) with 16 bit precision.

Signal Processing

The eddy current sensor generates significant 250Hz magnetic fields that are picked up by the magnetometers. In addition, in spite of the distance from Nomad, there was still significant vehicular noise interference. Fortunately, since the vehicle speed was approximately 30cm/s and the sensor footprint is approximately 20cm, signals of interest are less than 10Hz, while most of the noise is at higher frequencies. Low pass filtering with a 10Hz cut-off frequency and down-sampling to 20Hz improves the data and reduces its volume.

The top magnetometer (low pass filtered) readings are used to infer the primary field (geomagnetic field and common mode low frequency vehicular interference field emissions) measured by the bottom magnetometer. Thence the secondary magnetic field due to a ferrous object can be deduced, and orientation independent quantities (such as magnitude) computed from it. Furthermore, low frequency common mode interference (that cannot be removed with low pass filters) is rejected.

Assuming a uniform magnetic field (such as the Earth's), the fields *measured* (as opposed to the actual fields; the magnetometers response to a field may change with time) by the top and bottom 3-axis vector sensors are related by a rotation, scaling and displacement:

$$\vec{B}_{bottom} = \tilde{S} \cdot \tilde{R} \cdot \vec{B}_{top} + \vec{D}$$

$$\tilde{S} = \begin{bmatrix} s_1 & 0 & 0 \\ 0 & s_2 & 0 \\ 0 & 0 & s_3 \end{bmatrix}$$

$$\tilde{R} = rotation \quad matrix$$

The rotation reflects the arbitrary orientation of the sensors with respect to each other. The scaling and offset arise from differences in the sensor scale factors and zero offsets.

Thus, the quantities

$$\vec{B} = \vec{B}_{bottom} - (\tilde{S} \cdot \tilde{R} \cdot \vec{B}_{top} + \vec{D})$$

$$B = \|\vec{B}\|$$

$$A = \angle(\vec{B}_{bottom}, \tilde{S} \cdot \tilde{R} \cdot \vec{B}_{top} + \vec{D})$$

represent respectively the secondary field *as measured* by the bottom magnetometer (but with any zero offsets removed), its magnitude, and the angle between the bottom field and the ambient field as it would be measured by the bottom sensor. If the zero-offsets are not cancelled, the quantities **A** and **B** could be nonzero even in the absence of a secondary field, and *not* be invariant under sensor rotations.

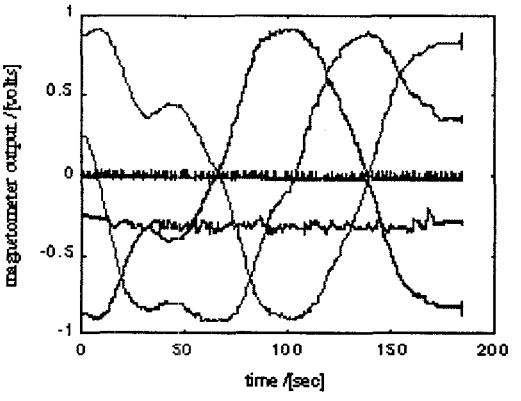

Figure 4 Output from upper and lower magnetometers (Atacama Desert location)

Calibration data was obtained both in the Atacama desert (Figure 4) and a slag heap in Pittsburgh, with the rover dragging the sensor platform along a curved path relatively free of ferrous objects (the Pittsburgh slag heap contained many small pieces of iron; fortunately they appeared to have minimal magnetic signatures). The transformation matrices and displacement vector were solved for using least squares estimation.

$$\tilde{R}=\begin{bmatrix}-1.00 & -0.003 & -.001\\ 0.00 & -1.00 & -0.03\\ 0.00 & -0.03 & 1.00\end{bmatrix}\quad \tilde{S}=\begin{bmatrix}0.98 & 0 & 0\\ 0 & 1.00 & 0\\ 0 & 0 & 0.99\end{bmatrix}\quad \vec{D}=\begin{bmatrix}-0.23\\ 0.01\\ -0.01\end{bmatrix}$$

Figure 5 Magnetometer transformation parameters in Atacama Desert (matrices are unitless, offset is in volts)

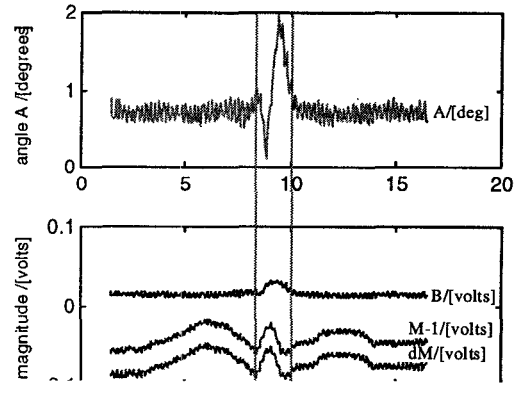

Figure 6 Magnetic meteorite signatures

Figure 6, computed from data obtained by dragging the sensor over a large meteorite in the Atacama (Carraweena), using the transformation parameters in Figure 5, illustrates the advantage of this technique over traditional techniques using the quantities:

$$dM = \left\|\vec{B}_{bottom}\right\| - \left\|\vec{B}_{top}\right\|$$

$$M = \left\|\vec{B}_{bottom}\right\|$$

where **dM** is the difference in the measured magnitudes of the top and bottom fields, and **M** is the measured magnitude of the bottom field.

The central rectangle indicates the signals due directly to the meteorite's magnetic field. The middle peak due to the (meteorite) secondary field is clearly visible. However, both M and dM also have large peaks, on either side of the central one, caused by the pitching of the platform as it is moved over the meteorite. A large zero level offset (approximately 0.2 volts, cf Figures 4 and 5) in the bottom magnetometer is responsible for this sensitivity to orientation in the computed values of **M** and **dM**. The calibration procedure outlined above eliminates this flaw and does not require known magnetic fields or other specialized facilities. Longer runs dragging the sensors along curved paths and up and down slopes confirmed this.

Furthermore, signal level of B does not depend on the orientation of the secondary field with respect to the primary field, as does M or dM, and has better noise rejection.

Ideally A and B would be both zero in the absence of a secondary field. However, not all vehicular interference is common to both sensors. Furthermore, the three vector sensors in each magnetometer unit are not strictly orthogonal, but may deviate slightly (< 0.2°). Therefore, there should also be a slight shear component to the transformation equation. Nevertheless, it is small, and estimating it along with the other paramaters in the presence of noise turned out to be unstable.

Observational Data

Data was collected with real meteorites (olive pip sized iron samples to larger stony samples) both in the Atacama and in Pittsburgh, with the vehicle travelling at approximately 30cm/s. Differing geomagnetic fields and mineralogy affected the results. Additionaly, the complete failure of one magnetometer and the partial failure of another in the Atacama necessitated separate calibration for each location, and indicates the probable necessity of multiple recalibration of the system if deployed for extended periods of time.

Sensor responses (processed) to a large stony meteorite (Carraweena) are shown in Figures 7, 8 and 9. The different geomagnetic field strengths (60,000nT in Pittsburgh, 30,000nT in the Atacama) and declinations might explain the different magnetomer responses. In addition, there were many iron pieces in the Pittsburgh slag heap that affected the sensors. In comparison to the field data, the laboratory magnetometer data (obtained by manually moving the meteorite under the sensors) is exceptionally noise free. However, there is a significant DC offset, probably due to the large iron content in the laboratoy building.

Figures 10 and 11 show the sensor response to a

small iron meteorite (the sample with the smallest magnetic signature, but largest metal detector signature) and the Kulnine stony meteorite (no metal detector response).

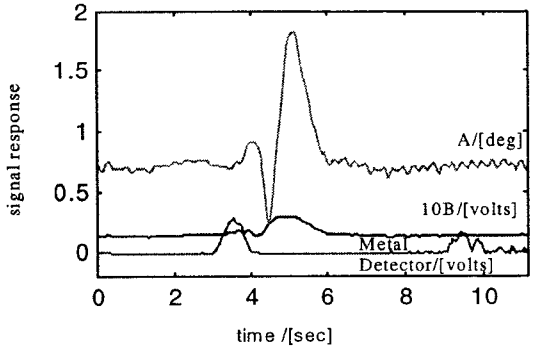

Figure 7 Carraweena meteorite, Atacama desert

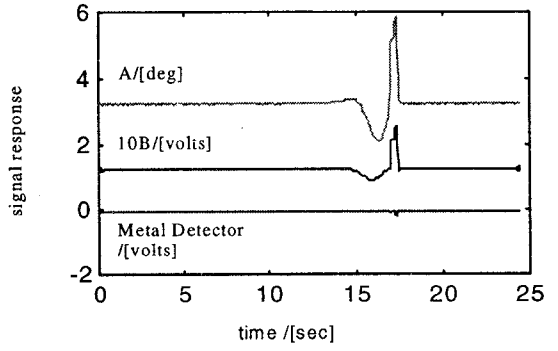

Figure 8 Carraweena meteorite, Pittsburgh laboratory

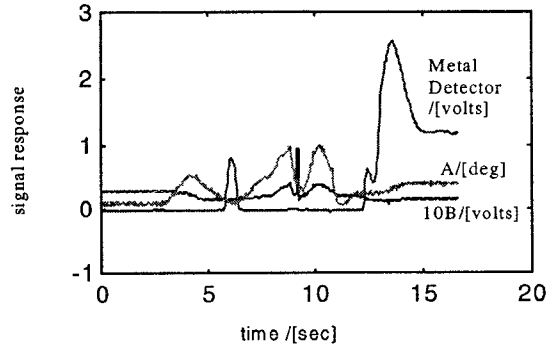

Figure 9 Carraweena meteorite, Pittsburgh slag heap

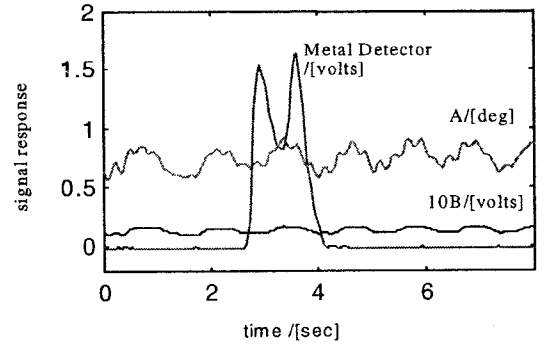

Figure 10 Small iron meteorite, Atacama Desert

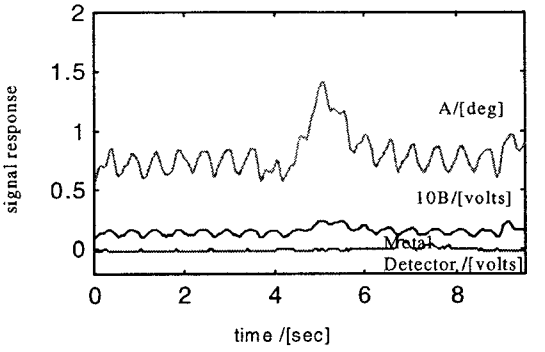

Figure 11 Kulnine meteorite, Atacama desert

Pattern Recognition and Sensor Fusion

The results show that a simple threshold-crossing detector is less than adequate for autonomous recognition of meteorite electromagnetic signatures. An adaptive thresholding algorithm produced tolerable results but still gave a high number of false positives. Because of the large variation in the signatures, even for the same sample, it is questionable whether a single pattern classifier could be built to successfully resolve all cases.

Data from multiple sensors is correlated, and can be combined to increase the certainty (or uncertainty) of a find. For example, a magnetometer confirmation of a metal detector event decreases the likelihood of it been noise. Similarly, the output from multiple classifiers operating on the same data stream can be combined to increase certainty.

A principled approach is to use the formalism of Bayes networks to integrate data from multiple sensors and pattern classification algorithms with domain specific knowledge about the problem, including the statistical likelihood of finding meteorites at a given location in the first place.

For example, the following network appears to capture the statistical relationships relevant to a metal detector and magnetometer system:

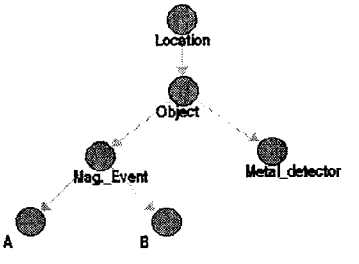

Figure 12 Bayes network for rock/meteorite classification

The probability of a ferrous object being in the sensor footprint at any instant is dependant on the location of the sensors (Pittsburgh or the Atacama in this example). In turn, the existance of an object underneath the sensors

affects the probability of the metal detector output exceeding some threshold. Likewise for the magnetometer signals. Thus, whenever a detection event occurs (A,B or the metal detector output exceeding some threshold), the posterior probability of an object been located under the sensors can be evaluated using Bayes rule.

Current work in progress is to implement this, along with multiple classifiers to operate simultaneously on the data streams.

Conclusions

The sensor configuration developed here is able to accommodate both sensors on a single platform and resolves the vehicular noise and calibration issues mentioned earlier. The magnetometers can be calibrated in the field and the output processed to obtain quantities that are independent of orientation, yet sensitive to localized fields produced by objects near the sensors. The value of this system was proven in the field when the lower magnetometer developed a large zero offset causing naïve computations of the lower field magnitude to depend strongly on sensor orientation.

Signal quality could possibly be further improved by removing periodic interference (cf Figures 10 and 11). However, initial trials were not encouraging as the interference has multiple harmonics and removing them all adversely affected the signal.

From the robotic perspective, the ability to recalibrate sensors in the field is essential. Long duration missions are likely to experience sensor changes. Normally, special facilities would be needed. Without calibration, sensor outputs will vary unacceptably as sensors are moved over rough terrain, with a high number of false positive results.

The combined pulse induction metal detector and magnetometer system is effective for detecting meteorites. The sensors complement each other well, the former responding most strongly to iron meteorites, and the latter to stony meteorites.

The metal detector proved to be a particularly valuable yet troublesome sensor. When deployed manually it was sensitive to all the sample meteorites, and was used to discover two pallasite (stony iron meteorites) specimens in a known impact site at Imilac in Chile. However, results from a robotic deployment are less encouraging. The unit was sensitive to vehicular emissions, and would occasionally behave unpredictably for no apparent reason.

If the robot was travelling at excessive speed, the metal detector was unable to respond to metal objects within its footprint. Search speed is limited by the device response time, to less than 30 cm/s for the model used by us.

Future work will be to integrate the sensors with the robot navigation sensors. The odometry logs are of particular importance. By associating a position with sensor readings, data taken at different times from different sensors at the same point can be more effectively compared. Advanced pattern recognizers will be applied to the data streams and the results combined through the formalism of a Bayes network to obtain improved statistical estimates of the likelihood meteorite detection.

Acknowledgements

This project was supported by NASA through grants NAGW-3863 and NAGW-1175.

I am indebted to the staff of the mine detection group at the Defense Research Establishment Suffield (DRES) in Canada for their invaluable assistance, advice and loan of equipment.

Professor Bill Cassidy of the University of Pittsburgh loaned the meteorite samples used in this study and, as a veteran meteorite searcher and participant in the ANSMET program provided much information on the distribution and properties of meteorites, and the manner in which human teams search for them.

Finally, the success of the Nomad field trials was the result of teamwork by many people. I would like to thank all the participants for their efforts.

References

[1] Heide, Fritz, "Meteorites", University of Chicago Press, 1964

[2] Wasson, John T., "Meteorites: classification and properties", Springer-Verlag, 1974.

[3] McFee, J.; Das, Y.; and Ellingson, R., "Locating and Identifying Compact Ferrous Objects", *IEEE Transactions on Geoscience and Remote Sensing*, Vol. 28, No. 2, March 1990.

[4] McFee, J.; and Das, Y.; "Determination of the Parameters of a Dipole by Measurement of the Magnetic Field", *IEEE Transactions on Antennas and Propagation*, Vol. AP-29, No. 2, March 1981.

[5] Faugeras, Olivier, "Fundamentals in Computer Vision: an advanced course", Cambridge University Press, 1983

[6] Pearl, J., "Probabilistic Reasoning in Intelligent Systems: Networks of Plausible Inference", Morgan Kauffman, 1988.